LMG 2 – Advancing Quantum Dynamics in Atomistic Simulations of Molecular Systems, Materials, and Interfaces

Hannah Bertschi, Krystof Brezina, Jorge Castro, George Trenins, and Mariana Rossi

Max Planck Institute for the Structure and Dynamics of Matter, Hamburg, Germany

Vibrational Spectroscopy

Tip-Enhanced Raman Spectroscopy

Led by Krystof Brezina

TERS combines the chemical specificity of Raman spectroscopy and the molecular resolution of scanning-probe microscopy and allows imaging atomic/molecular motion at sub-nanometer resolution [1] on conductive surfaces (Fig. 1).

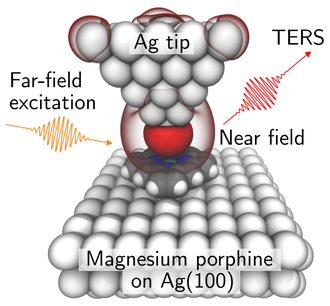

Figure 1: Principles of TERS spectroscopy. The incoming far field (orange) induces a local plasmon resonance in the atomically sharp tip, leading to an intense near field (red surface) and a localized enhancement of Raman scattering (red) from the junction region.

- Chemical enhancements from the surface can significantly contribute to the TERS signal of adsorbed molecules.
- Previously, we proposed a first-principles methodology for the calculation of non-resonant TERS based on density-functional perturbation theory for clusters [2]; now we extend this method to periodic systems, based on a finite-field framework, which allows the simulation of more realistic experimental conditions (Fig. 2).

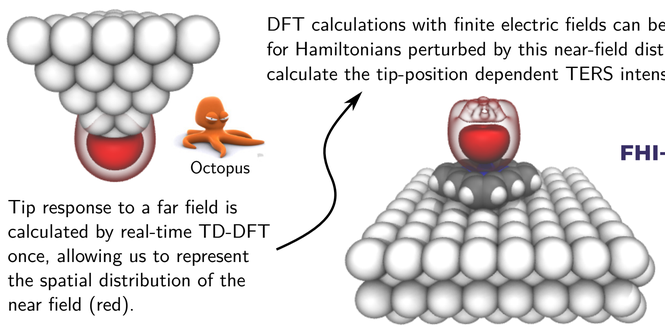

Figure 2: The workflow of the first-principles TERS calculation on periodic metals. The tip near field is represented by the red isosurface.

Magnesium Porphine on Ag(100)

We applied our method to simulations of magnesium porphine on Ag(100), reaching excellent agreement with experimental data [1]. We found that the surface is a key factor in shaping the TERS images. A comparison of experimental and computational TERS images of a selected vibrational mode is shown in Fig. 3.

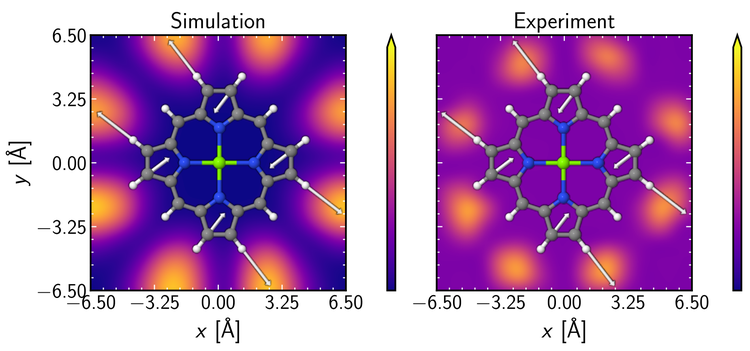

Figure 3: TERS imaging of the asymmetric hydrogen stretch in magnesium porphine on Ag(100). Left: calculation using the proposed methodology. Right: experimental data [1]. The molecular structure and the mode vector are shown in both panels.

Outlook: Coupling the workflow to path-integral molecular dynamics (PIMD) simulations, to calculate TERS signals including anharmonic nuclear quantum effects (NQE).

Vibrations with Quantum Nuclei

Led by Jorge Castro

NQE have a strong impact on features such as line shapes and temperature-dependent frequency shifts in vibrational spectra. The centroid molecular dynamics (CMD) family of PIMD methods comprises state-of-the-art approaches for including NQE into atomistic simulations (Fig. 4). Elevated-temperature path-integral coarse graining (T_e-PIGS) [3] mitigates the artefacts affecting high-frequency modes (Fig. 4c), but relies on machine-learned (ML) mean-field forces for driving the vibrational dynamics. We introduce a partially adiabatic variant, PA-T_e-CMD, which computes such forces on the fly and can be used when ML training data are scarce.

Quantum Nuclei (contd.)

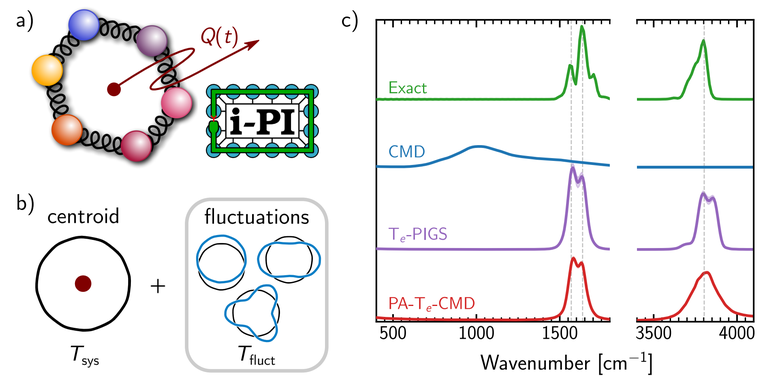

Figure 4: (a) NQE are captured by PIMD, which replaces each atom by P replicas connected by harmonic springs (a ring polymer). Vibrational spectra are computed from the dynamics of the ring-polymer centroids, as implemented in i-PI [4]. (b) In centroid molecular dynamics (CMD), the centroids evolve at the temperature T_{sys} under mean-field forces from the fluctuation modes. When the temperature of the fluctuations $T_{fluct} = T_{sys}$, CMD can give rise to distorted spectra. In elevated-temperature CMD, $T_{fluct} > T_{sys}$, which suppresses the artefacts. (c) IR spectra of a water molecule at 50 K from different imaginary-time path-integral methods. The exact spectrum is shown for reference, with vertical dashed lines as visual guides.

Methylammonium Lead Iodide

We used CMD methods to simulate different polymorphs of the hybrid perovskite MAPI. Both T_e-PIGS and PA-T_e-CMD significantly reduce artefacts and produce reliable vibrational spectra accounting for NQE.

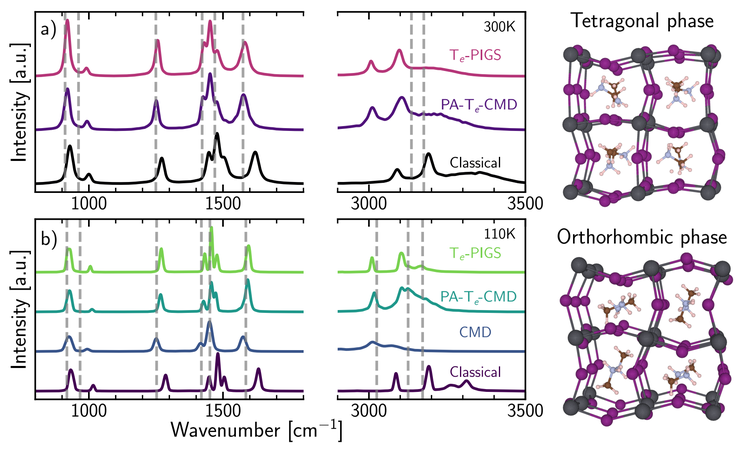

Figure 5: Vibrational density of states (VDOS) of MAPI computed using T_e-PIGS, PA-T_e-CMD, CMD, and classical MD. (a) VDOS in the tetragonal phase at 300 K and (b) VDOS in the orthorhombic phase at 110 K. T_{fluct} was set to 500 K in both cases. Experimental IR lines (dashed grey) are shown for reference [5].

Nonadiabatic Dynamics

Nuclear Motion with Electronic Friction

Led by George Trenins

Nonadiabatic effects at metallic interfaces (Fig. 6) can be cast as electronic friction (EF), parametrized by the position-dependent diffusion coefficient $\boldsymbol{\Sigma}(\mathbf{R})$ and the time-dependent memory kernel $K(t)$, both available from DFT calculations [6].

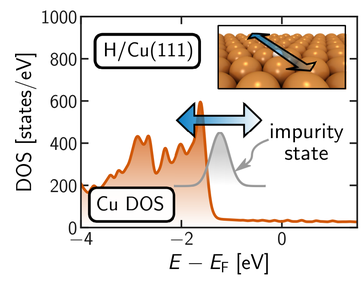

Figure 6: The motion of a hydrogen atom on Cu(111) (inset) changes the electronic structure around the Fermi level, namely, the energy of an "impurity state" and its coupling to the metal states. The dynamical changes induced by the motion excite electron–hole pairs, opening a new energy dissipation channel for the adsorbate. In the limit of weak nonadiabatic coupling, the dissipation is described by EF.

To account for NQE, we include EF into ring-polymer molecular dynamics (RPMD). This is accomplished by mapping onto an "explicit" harmonic bath (Fig. 7a), from which we derive the ring-polymer generalized Langevin equation (GLE) [7].

Figure 7: (a) Ring polymer (RP) with four bath modes; same-colour modes are connected by springs that are omitted for clarity. (b) Mean-field forces act on RP fluctuation modes and modify static properties. (c) Dissipative and stochastic forces are fully determined by $K^{(n)}$ and $\boldsymbol{\Sigma}^{(n)}$. The latter are simple linear combinations of $\boldsymbol{\Sigma}$ for different RP replicas.

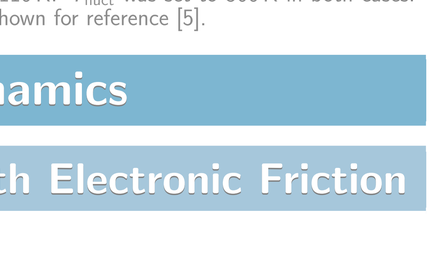

The GLE comprises tunnelling-suppressing mean-field forces (Fig. 7b), as well as dissipative and stochastic forces (Fig. 7c):

$$\sum_n -\int^t \boldsymbol{\Sigma}^{(n)}(\widetilde{\mathbf{R}}_t) K^{(n)}(t-t') \boldsymbol{\Sigma}^{(n)}(\widetilde{\mathbf{R}}_{t'})^{\mathsf{T}} \dot{\widetilde{\mathbf{R}}}_{t'} \,\mathrm{d}t' + \boldsymbol{\Sigma}^{(n)}(\widetilde{\mathbf{R}}_t)\zeta^{(n)}(t).$$

The diffusion coefficients $\boldsymbol{\Sigma}^{(n)}$ and friction kernel $K^{(n)}$ are associated with the n-th RP normal mode (Fig. 4b). They are simple transforms of $\boldsymbol{\Sigma}$ and K [7].

Electronic Friction (contd.)

We propagate RPMD+EF using an efficient algorithm [7], to compute reaction rates as $k = k_{\mathrm{QTST}} \times \kappa(t_p)$ (Fig. 8).

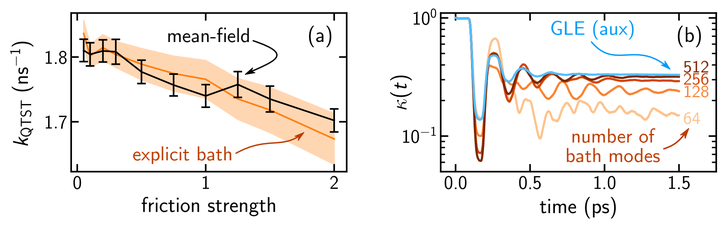

Figure 8: (a) Quantum transition-state theory (QTST) rates. Using mean-field forces, we describe the suppression of quantum tunnelling at a much reduced cost compared to the explicit-bath representation. (b) Dynamical transmission coefficients extending to the plateau time, t_p. We use auxiliary variables to propagate the GLE. Here, the dissipative dynamics converges with only 5 pairs of variables.

The method gives deep insight into the interplay of NQE and EF in the diffusion of hydrogen on Cu(111).

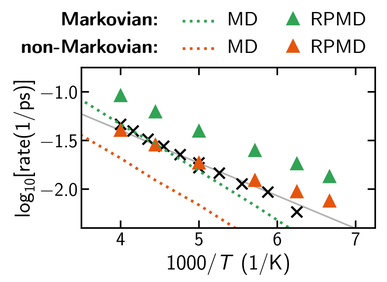

Figure 9: The black crosses show the escape rates for H from the hcp hollow on the Cu(111) surface, measured by ^{3}He surface spin echo spectroscopy. These are compared with classical (MD) and quantum (RPMD) simulation results for a 1D model parametrized by DFT energies. The Markovian simulations set $K(t) = \delta(t)$, and the non-Markovian simulations use the ab initio memory kernel.

Nuclear Motion with Ehrenfest Forces

Led by Hannah Bertschi

Ehrenfest dynamics can describe nonadiabatic effects even in the strong coupling limit, where electronic friction fails. Observables are computed either from a single trajectory (STEF) initialized at a specially chosen geometry, or by averaging over multiple trajectories (MTEF) [8], sampled from the Wigner distribution.

Spectrum and Sampling of the Water Dimer

In practice, the Wigner distribution must be approximated, e.g., using the quantum harmonic approximation (Fig. 10). The spread in the sampled geometries leads to stark differences between STEF and MTEF.

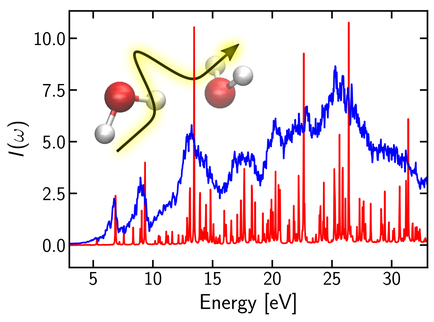

Figure 10: The water dimer is excited by a δ-like electric pulse [8] (glowing arrow). The vibronic spectrum is calculated from the Fourier transform of the resulting dipole-moment fluctuations. The STEF result (in red) was obtained from a trajectory initialized at the equilibrium geometry. The MTEF result (in blue) was obtained by averaging over 170 trajectories sampled from harmonic initial conditions at 50 K.

However, the internal rotation and the hydrogen-bond coordinate are poorly described by the harmonic approximation. Therefore, we employ quantum thermostatting (QT) [9] to incorporate anharmonic effects.

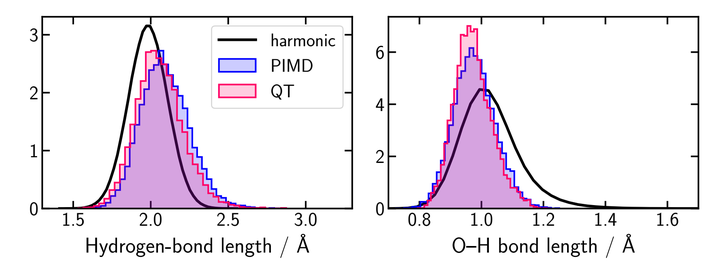

Figure 11: Comparison of the positions sampled using QT to the exact quantum (PIMD) reference. For both the hydrogen-bond length and the covalent O—H bond, the harmonic approximation deviates significantly from the quantum reference, whereas QT captures the distribution essentially exactly.

Our ongoing research on benzene and water clusters lays the groundwork for studying anomalous energy transfer at the water–graphene interface and similar systems.

References

[1] Y. Zhang *et al.*, Natl. Sci. Rev. **6**, 1169 (2019).
[2] Y. Litman *et al.*, J. Phys. Chem. Lett. **14**, 6850 (2023).
[3] F. Musil *et al.*, J. Chem. Phys. **157**, 181102 (2022).
[4] Y. Litman *et al.*, J. Chem. Phys. **161**, 062504 (2024).
[5] G. Schuck *et al.*, J. Phys. Chem. C **122**, 5227 (2018).
[6] C. L. Box *et al.*, Electron. Struct. **5**, 035005 (2023).
[7] G. Trenins and M. Rossi, arXiv:2412.15014 (2024).
[8] K. Lively *et al.*, J. Phys. Chem. Lett. **12**, 3074 (2021).
[9] M. Ceriotti *et al.*, Phys. Rev. Lett. **103**, 030603 (2009).